Investigating Chemistry of Metal Dissolution in Amine-Thiol Mixtures & Exploiting it towards Benign Ink formulation for Metal Chalcogenide Thin Films

Xin Zhao,† Swapnil D. Deshmukh,† David J. Rokke, Guanghui Zhang, Zhenwei Wu, Jeffrey T. Miller, and Rakesh Agrawal*

Davidson School of Chemical Engineering, Purdue University, 480 Stadium Mall Drive, West Lafayette, IN 47907-2100, United States

ABSTRACT: Solution processing of metal chalcogenides using elemental metals dissolved in an amine-thiol solvent mixture has recently received a great deal of attention for the fabrication of thin-film optoelectronic devices. However, little is known about the dissolution pathway for metallic precursors in such mixtures. To exploit the full potential of this method, it is essential that a detailed understanding of the dissolution chemistry be developed. In this study, we use several characterization techniques to examine these solutions and then propose reaction mechanisms for In and Cu dissolutions in a hexylamine-1,2-ethanedithiol mixture. These dissolutions are rather found to be reactions resulting in metal oxidation with co-evolution of H_2 forming bis(1,2-ethanedithiolate) indium (III) in the case of indium dissolution and high nuclearity Cu (I) thiolate compounds in case of copper dissolution. This understanding allowed us to address the issue of toxicity and corrosivity associated with amine-thiol solvent by utilizing it as reactant rather than a solvent for ink formulation. Here, we demonstrate a new approach whereby metal complexes formed by dissolving range of metals including Cu, In, Zn, Sn, Se and Ga with Se in amine-thiol solution can first be isolated by evaporation of the precursor solution and then dissolved in variety of weakly coordinating organic solvents to provide benign and stable solution, free of unreacted amine and thiol, for thin film fabrication of various chalcogenide semiconductors. We utilize this new approach to demonstrate fabrication of $CuIn(S,Se)_2$ solar cells using DMSO as a fabrication solvent.

1. Introduction

The scalable and safe production of high-performance solution processed metal chalcogenide films has been an important thrust in the materials research community, potentially enabling a wide range of applications in solar cells, thermoelectrics and transistors. Metal chalcogenide thin film solar cells that rely on the sequential deposition of layers could especially benefit from solution processing to realize high throughput and hence the low-cost manufacturing. Chalcopyrites $CuIn(S,Se)_2$ (CISSe) and $Cu(In,Ga)(S,Se)_2$ (CIGSSe) are promising materials in high performance photovoltaics owing to their high absorption coefficient, bandgap tunability, long term stability and high defect tolerance[1]. Vacuum-deposited $CuInSe_2$ and $CuInGaSe_2$ (CIGSe) films exhibit efficiencies of up to 15.0%[2] and 22.9%[3] in laboratory-scale devices respectively. Solution-based approaches allow for printable semiconductor thin films using spray, slot-die or micro-gravure coating techniques on rigid or flexible substrates at relatively low temperatures using high-throughput technologies like roll to roll manufacturing, which is expected to be a commercially viable alternative to traditional low throughput high-vacuum deposition methods.

Among all solution-based approaches, a great deal of attention has been received by the direct dissolution of metals and chalcogens into a molecular precursor solution, which requires few synthesis steps and affords the opportunity for large-scale cost-effective processing of high-quality semiconductors. However, several challenges still remain in such formulations. First, many widely utilized solvents can only dissolve limited metal precursors such as metal salts (chlorides[4,5], nitrates[6,7], acetates[8], and acetylacetonates[9,10]) and oxides[10–12]. These precursors exhibit metal coordination with elements like O, C, Cl, and N which can remain in the chalcopyrite films, potentially interfering with the formation of a high-quality semiconducting film. Second, incorporating Se into the films at moderate conditions is difficult for most of the reported molecular solution-based techniques. To tackle these challenges, hydrazine has been utilized to dissolve precursors such as Cu_2S, In_2Se_3, and Ga with elemental Se to yield inks for film fabrication.[13] Hydrazine-based solution processed CISSe and CIGSSe devices have been successfully demonstrated with efficiencies up to 12.2%[14] and 17.3%[15] respectively. However, the high toxicity and explosive nature of anhydrous hydrazine limit its practical application in industrial processes. Therefore, it is of great importance to seek a safer approach for high-quality chalcopyrite-based thin films while minimizing elemental impurities.

In pursuing precise stoichiometric control and clean film deposition, it was postulated that ideal precursors for solution processed metal chalcogenide thin films should be prepared using elemental metals and chalcogens. Recently, the amine-thiol solvent system was found to possess remarkable solvent ability for metals (e.g. Cu, In, Zn, Sn)[16–18] and elemental Se[19,20] at room temperature. The resulting amine-thiol precursor solutions have been applied to deposit $Cu_2ZnSnSe_4$[17,21], $(Cu_{1-x}Ag_x)_2ZnSn(S,Se)_4$[22], $Cu_2BaSnS_{4-x}Se_x$[23], $Cu(In,Ga)Se_2$[16], and SnS[18] films. Notable efficiencies of 9.5% and 8.02% were presented by Zhao et al. and Yang et al. for $Cu(In,Ga)Se_2$ and

$Cu_2ZnSnSe_4$devices.[16,21] Despite the excellent solvent capabilities and promising device performances, some items must be addressed for the amine-thiol system to attain broader applicability. 1) The amine-thiol system is capable of dissolving a variety of other metal sources including metal oxides[24], metal chalcogenides[25] and metal salts[26,27]. However, few studies have been dedicated to investigating the dissolution mechanisms of such precursors. Dissolution of metallic precursors provides a simpler system (i.e. free of anionic species) to investigate the mystery of this "universal" solvent system. In addition, it is necessary to study the structure and properties of the metal complexes formed to enable the design and optimization of the device fabrication process. 2) Amine-thiol cosolvents are corrosive and may be toxic as evidenced by their precursor dissolution ability. During experimentation, it was found that this mixture poses a material compatibility challenge. It corrodes many materials such as metals, metal oxides, silicone and nitrile. Materials like glass, polypropylene, polytetrafluoroethylene, and stainless steel, are the only ones we've found to be compatible with it. This causes special requirements for the handling equipment and could potentially increase the manufacturing costs if brought to industrial-scale application.

To address the above issues, the dissolution reactions of Cu and In metals in a hexylamine (HA)/1,2-ethanedithiol (EDT) cosolvent were examined. Metal thiolate anions counterbalanced by ammonium cations are identified using X-ray absorption spectroscopy (XAS), mass spectrometry, and ^1H and ^{13}C NMR. The gaseous product generated during dissolution is also analyzed by thermal conductivity measurements. The overall reactions for the dissolutions of Cu and In in HA-EDT mixture are proposed and the resulting Cu and In thiolate salts formed in these reactions are isolated by evaporating the HA-EDT precursor solutions for further film fabrication. These isolated metal thiolate salts are found to be soluble in several benign solvents such as dimethyl sulfoxide, dimethyl formamide, 2-methoxyethanol, acetonitrile etc. that possess more weakly coordinating ability compared to organic amines or thiols. In one of the experiments, the isolated metal thiolates/complexes from Cu, In and Se inks are dissolved in dimethyl sulfoxide (DMSO) to produce new molecular precursor solutions. Using this ink, a CISSe thin film solar cell with efficiency of 9.03% is demonstrated for a total area of 0.472 cm^2. This new approach enables us to use amine-thiol solution as a reactant for metal thiolate formation, which can avoid the utilization of amine-thiol as a solvent during film processing, ensuring safe, low-cost and scalable fabrication. In addition to Cu and In, it was found that other metals such as Zn, Sn, and Ga with Se dissolved in amine-thiol solvents can be isolated by evaporating the resulting solution and then dissolved in various weakly coordinating benign solvents. This approach can be generalized for the fabrication of a wide range of metal chalcogenide based thin film devices. The solvents identified here provide a number of low-toxicity alternatives for the solution processing of metal chalcogenide materials, and their weakly coordinating nature helps to achieve high quality, clean film fabrication.

2. Experimental Section

Materials: Ga pellets (6 mm dia, 99.99999% metals basis) were purchased from Alfa Aesar. Cu (40-60 nm, >99.5% metal basis containing 2% oxygen), In (100 mesh, 99.99% metal basis), Zn (<50 nm, >99% metal basis), Sn (<150 nm, >99% metal basis), Se (100 mesh, 99.99% metal basis), Hexylamine (99%), 1,2-ethanedithiol (>98%), Dimethyl sulfoxide (99.9%), N,N-dimethylformamide (99.8%), Acetonitrile (99.8%), 2-methoxyethanol (99.8%), Tetrahydrofuran (>99.9%) and Formamide (>999.5%) were purchased from Sigma-Aldrich. All chemicals were used as received except for Ga pellets, which are scraped with a razor blade to remove a possible oxide layer on the surface prior to dissolution.

HA-EDT precursor solution preparation: 0.1 M Cu solution was prepared by dissolving 3.5 mmol of Cu nano-powder (40-60 nm particle size) in 31.81 mL HA and 3.18 mL EDT with continuous stirring for several days. Similarly, 0.4 M In solution was prepared by dissolving 3.5 mmol of In in 7.96 mL HA and 0.796 mL EDT with continuous stirring for several days. 0.5 M Se solution was prepared by dissolving 1.25 mmol Se in 2.27 mL HA and 0.227 mL EDT with continuous stirring for a few minutes. All solutions were prepared at room temperature in a N_2 atmosphere glovebox with oxygen and H_2O concentration less than 0.1 ppm.

Metal thiolate Isolation: After complete dissolution, the 0.1 M Cu-HA-EDT solution (35 ml) was transferred to a 100 mL round bottom flask connected to a Schlenk line apparatus with a liquid nitrogen cold trap. Vacuum was pulled in the Schlenk line with the round bottom flask isolated until the system reached pressures below 120 mtorr. The solvent was then evaporated at room temperature under vacuum. At ~ 7 min, pale-yellow solids started to form in the flask. At ~ 11 min, all the content was solidified. Then the flask was heated to ~ 35 °C to slowly melt the mixture into a yellow liquid. At ~ 20 min, the mixture had melted, and the flask was gradually heated up to ~ 55 °C. At ~ 42 min, a highly viscous gel was left in the flask and the temperature was raised up to ~ 60 °C. The evaporation process was stopped after ~58 min. The final isolated copper complex was a thick paste and golden in color.

Similarly, 0.4 M In-HA-EDT solution (8.75 ml) was transferred to a 100 mL round bottom flask and connected to the Schlenk line. The solvent was first evaporated at room temperature under vacuum, and then the flask was gradually heated up to ~ 70 °C. The evaporation was stopped at ~46 min and the final indium complex isolated in this process was white with a more powdery consistency than the copper complex. For Se complex isolation, 0.5 M Se-HA-EDT solution (2.5 ml) was transferred in a 15 mL round bottom flask connected to the Schlenk line. The solvent was evaporated at room temperature under vacuum until a dark red, viscous gel was formed. Then the flask was heated to ~ 42 °C and the evaporation was stopped at ~13 min. The final Se complex isolated in this process was dark red in color with dryer consistency than the copper complex.

Cu/In thiolate precursor mixture for CISSe film fabrication was prepared by combining Cu-HA-EDT and In-HA-EDT solutions with the atomic ratio [Cu]:[In] = 0.95:1 and evaporating it using a similar evaporation procedure to that described above.

Metal thiolate DMSO precursor solution preparation: The isolated Cu thiolate, In thiolate, Se complex, and Cu/In thiolate precursors from evaporation process were dissolved separately in DMSO with continuous stirring for several hours to form 0.5 M solutions. The solution for film fabrication was formed by mixing Cu/In thiolate DMSO solution and Se DMSO solution with In species concentration of 0.5M and the atomic ratio ([Cu]+[In]): [Se] = 1: 0.1. This solution was transparent orange in color and remained stable for a few days. All solutions

were prepared at room temperature in a N_2 atmosphere glovebox with oxygen and H_2O concentrations less than 0.1 ppm.

Film fabrication: CISSe precursor film was spin-coated onto 1" × 1" molybdenum coated (~800 nm) soda lime glass substrate using the DMSO ink mentioned above for X-ray diffraction, Raman, SEM, and device fabrication. Spin-coating was performed in a nitrogen glovebox at 500 rpm for the first 5 sec followed by 1500 rpm for the next 25 sec. After each coating, the film was immediately annealed on a preheated hot plate at 330 °C for 5 min. This deposition step was repeated for 8-10 cycles to reach the desired film thickness. 10 nm of sodium fluoride was then deposited on top of the as-prepared precursor film by electron-beam deposition. The film was then selenized by exposing it to Se vapor in a graphite box (containing the sample and elemental Se pellets) at 500 °C for 30 min in a preheated tube furnace. Photovoltaic devices were completed by chemical bath deposition of ~ 50 nm cadmium sulfide (CdS), sputtering of ~ 80 nm intrinsic zinc oxide (ZnO) followed by ~ 220 nm indium tin oxide (ITO), and electron-beam deposition of Ni/Al grids. Each device on the film was separated by mechanically scribing, defining a total area of ~0.47 cm^2.

Characterization: The high-resolution mass spectrometry measurements were obtained on a Linear Trap Quadropole (LTQ) Orbitrap XL mass spectrometer (ThermoScientific Corporation) utilizing electrospray ionization (ESI). For In complex analysis, the isolated In thiolate was diluted in acetonitrile while for Cu complex analysis, Cu dissolved in HA-EDT solution (Cu:HA:EDT = 1:4:1 mole ratio) was diluted with acetonitrile (without performing an evaporation to isolate the complex) before injection into the mass spectrometer. The samples were infused into the mass spectrometer at a flow rate of 5 μL/min. The ESI spray voltage was operated at 4 kV and the resolution was set at 60,000. The vaporizing temperature was set at 275 °C.

X-ray absorption measurements were acquired at the Cu K edge (8.9790 keV) and In K edge (27.9400 keV) on the bending magnet beam line of the Materials Research Collaborative Access Team (MRCAT) at the Advanced Photon Source, Argonne National Laboratory. Measurements were made in transmission step-scan mode. The ionization chambers were optimized for the maximum current with linear response with 10% absorption in the incident ion chamber and 70 % absorption in the transmission detector. A third detector in series simultaneously collected a Cu or In metal foil reference spectrum with each measurement for energy calibration. Air and moisture sensitive reference compounds were loaded in an argon filled glove box. Liquid samples were prepared in a nitrogen filled glove box at 0.1 M metal concentration. Polymer cells were filled with liquid samples and sealed with a VCO face sealed fitting and Teflon O-ring inside a glovebox.[28] A solid $CuInS_2$ sample was prepared by pressing $CuInS_2$ nanoparticles, synthesized via previously reported procedure,[29] into a cylindrical sample holder consisting of six wells, forming a self-supporting wafer. The sample holder was placed in a quartz reactor tube sealed with Kapton windows by two Ultra-Torr fittings through which gas could be flowed. Argon was purged from the reactor with He and measurements were taken at room temperature in He. The fits of the Extended X-ray Absorption Fine Structure (EXAFS) were evaluated using Artemis software (Demeter 0.9.26).[30] The EXAFS coordination parameters were obtained by a least-squares fit in R-space of the k^3-weighted Fourier transform data from 3.0 to 11.0 $Å^{-1}$ and the first shell fits of the magnitude and imaginary parts were performed between 1.0 and 2.2 Å. The crystal structure of $CuInS_2$[31] was used as the fitting model for all samples, which fits the first coordination sphere of the EXAFS data well.

Nuclear Magnetic Resonance (NMR) spectroscopy was performed on Bruker AV-III-400-HD and Bruker DRX-500 instruments. Deuterated acetonitrile (CD3CN) and deuterated dimethyl sulfoxide (DMSO-d6) were used as solvents for In and Cu complex respectively for NMR analysis.

The composition of the gaseous products generated in the In-HA-EDT mixture reaction was determined using Micromeritics Autochem 2920 II, a fully automated chemisorption analyzer, coupled with an Agilent 5975C mass selective detector. N_2 was used as the carrier gas at a flow rate of 50 mL/min. The sample cell was then purged with N_2 for 40 min before the injection of the gas products. All the operational temperatures of the injection port and the detector were maintained at room temperature.

Thermogravimetric analysis (TGA) scans were performed on a TA Instruments Q50 system, in a flowing helium atmosphere and with a 10 °C/min ramp to 500 °C. Powder X-ray diffraction data were collected using Cu Kα radiation in a Rigaku SmartLab X-ray diffractometer. FEI Quanta 3D FEG Dual-beam SEM was used to obtain the micrographs of the films. Infrared spectroscopy measurements were conducted with Thermo Nicolet 6700 FTIR Spectrophotometer. The J-V characteristics were measured with a four-point probe station using Keithley 2400 series sourcemeter while the sample rested on a temperature-controlled stage at 25 °C. Illumination was provided by a Newport Oriel solar simulator with an AM1.5 filter set and calibrated to 1 sun intensity using a Si reference cell certified by NIST.

3. Results and Discussion

3.1 Dissolution Mechanism of Cu and In Metals in HA-EDT Solvent

3.1.1 In Thiolate Complex: In metal was dissolved in HA-EDT (10:1, v/v) under ambient temperature and pressure in a N_2-filled glovebox as described in experimental section. Evaporation of this solution was performed to isolate the In complex. Synchrotron-based X-ray Absorption Spectroscopy (XAS) was used to investigate the local structure of In in this complex. After completely dissolving In in HA-EDT solvent, the valance state of In is estimated using In K-edge X-ray absorption near edge structure (XANES) spectra (Figure 1). The edge energy and the shape of the XANES spectrum are affected by the valence state, the local coordination structure, and the electronic configuration of the absorbing atom. The edge energy of In-HA-EDT sample is higher than that of In foil and lower than that of In_2O_3. Furthermore, the edge energy and the shape of In-HA-EDT XANES spectrum match well to the $CuInS_2$ reference. These results indicate average oxidation state of In to be +3 in In-HA-EDT sample suggesting oxidation of In^0 metal to In^{3+} cation. After the In complex was separated from the HA-EDT solution by evaporation followed by dissolution in DMSO, the corresponding XANES spectrum (In-DMSO) remains the same, which suggests the local atomic environment of In remains stable in DMSO.

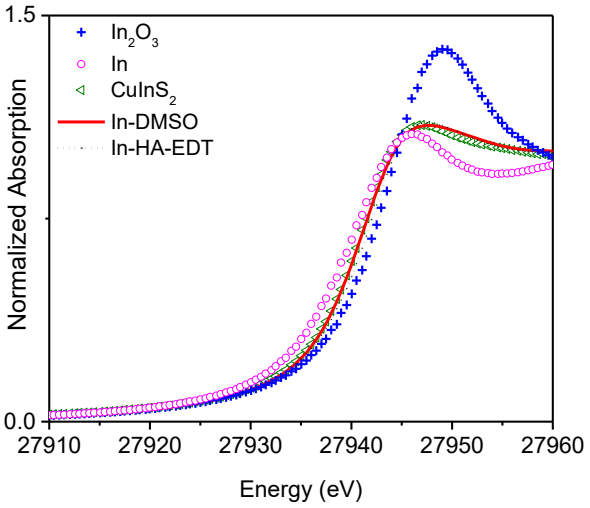

Figure 1. In K-edge XANES spectra for 0.1 M In in HA-EDT solution and 0.1 M In complex in DMSO solution along with In_2O_3, In foil, and $CuInS_2$ references.

Other local structure parameters, such as number and types of neighbor atoms and interatomic distances were obtained in the In-HA-EDT and In-DMSO samples by extended X-ray absorption fine structure (EXAFS) technique. The Fourier transforms of k^3-weighted In K-edge oscillation function for In-HA-EDT and In-DMSO are shown in Figure S1 of the supplementary information (SI). The first shell fittings are carried out to determine the bond distance (R), coordination number (C.N.) and the Debye-Waller factor (σ^2). The best fitting results are compared with the experimental spectra in Figure S1, and the fitting structural parameters are listed in Table 1. The average bond distances for In-HA-EDT and In-DMSO are 2.46 Å and 2.45 Å, respectively, which are close to the reference value of In-S bond in $CuInS_2$ of 2.46 Å.[32] Because sulfur has higher atomic number and radius than nitrogen/oxygen, In-S bond length is longer than In-N bond length of 2.10 Å[33] or In-O bond length of 2.18 Å.[34] The average coordination number obtained from the fit of In-HA-EDT is 4.0, and it holds constant in the In-DMSO solution, indicating coordination of 4 sulfur atoms with In^{3+} cation in both In-HA-EDT and In-DMSO samples.

Table 1. Structural parameters obtained from the best fits to In-HA-EDT and In-DMSO spectra at the In K edge

Sample	C.N.	R (Å)	σ^2 (Å^2)	E_0 (eV)
In-HA-EDT	4.0	2.46	0.005	1.0
In-DMSO	4.0	2.45	0.003	4.4

C.N.: Coordination Number, R: Interatomic distance, E_0: Shift in threshold energy, σ^2: Debye–Waller factor squared, S_0^2: Intrinsic loss factor, $S_0^2 = 1.0$.

Electrospray Ionization-Mass Spectrometry (ESI-MS) is used to further analyze the In-HA-EDT solution for its chemical composition. In the negative ion mode mass spectrum obtained for the In complex diluted in acetonitrile (Figure S2) the most significant species is found to be at m/z of 298.85 which corresponds to elemental composition of $C_4H_8InS_4^-$. Combined with the information obtained from XAS, bis(1,2-ethanedithiolate) indium (III), is proposed to form in the In-HA-EDT solution and is shown in Table 2. The second most abundant peak observed in negative mode mass spectra at m/z of 238.85 results from fragmentation of bis(1,2-ethanedithiolate) indium (III) molecule caused during ionization process (corresponding to $C_2H_4InS_3^-$). Positive ion mode ESI-MS revealed the presence of 3 amine ions, $C_6H_{16}N^+$, $C_{12}H_{28}N^+$, and $C_{18}H_{39}N_2^+$, at m/z = 102.13, m/z = 186.22, and m/z = 283.31 respectively (Figure S3). The proposed structures for these peaks contain primary, secondary, and tertiary amine ion are shown in Table S1.

Table 2. Molecular formulae and proposed structures for ions observed in negative mode high-resolution ESI-MS of In-HA-EDT complex

Measured m/z	Molecular Formula	Proposed Structures	Calculated m/z
238.8512	$C_2H_4InS_3^-$	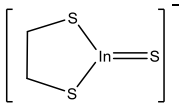	238.8514 (100%), 240.8472 (13.3%)
298.8542	$C_4H_8InS_4^-$	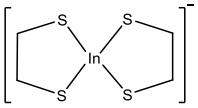	298.8548 (100%), 300.8465 (17.7%)

Calculated m/z column contains two highly abundant peaks for proposed structure with relative abundances in %.

Along with fragmentation, the ESI-MS analysis could also trigger some ionic interactions during the process of ionization. For validation of proposed structures in a liquid phase sample under ambient (non-reactive) conditions, NMR was performed on In-HA-EDT solution. The NMR sample was prepared by diluting isolated In thiolate in CD_3CN just before the analysis. The ^{1}H-NMR and ^{13}C-NMR data obtained from this analysis are presented in Figure S4 and Figure S5, respectively. For further confidence in peak assignments, 2D ^{1}H-^{13}CNMR was also performed and is shown in Figure S6. The peaks at δ 2.74 in ^{1}H-NMR and δ 34.6 in ^{13}C-NMR support the presence of bis(1,2-ethanedithiolate) indium (III) species in the solution. Additionally, there is no detectable NMR signal from any secondary or tertiary amine structures as proposed from ESI-MS data. This suggests the possibility of reactions occurring during the ionization process in MS analysis leading to the formation of secondary and tertiary amines.

3.1.2 Cu Thiolate Complex: XAS studies were also carried out at the Cu K-edge for the Cu-HA-EDT solution along with various references to gain insight into the electronic structures of copper centers. The collected XANES spectra are shown in Figure S7 while part of the spectra on energies near copper edge are summarized in Figure 2. The absorption edge energy (E_0) values of 8979.0 eV, 8980.2 eV, and 8980.6 eV for Cu in Cu foil, Cu_2O, $CuInS_2$ references, respectively were obtained from this analysis. CuO reference for Cu (II) exhibits a weak pre-edge transition at around 8977.5 eV, and a rising-edge transition at 8983.5 eV. The low energy, low intensity pre-edge feature is due to the 1s electron excitation into the Cu-centered 3d-hole, which is not observed for Cu (I) species. The edge of Cu-HA-EDT sample occurred at 8980.5 eV, and no pre-edge transition was observed in the spectrum. Therefore, the results indicate that Cu^0 metal was oxidized to Cu^+ in HA-EDT solution. The

Cu K-edge XANES spectrum of Cu-DMSO sample shows similar absorption edge features (E_0 = 8980.1 eV with no pre-edge transition), consistent with the same Cu^+ valance state and similar coordination environment.

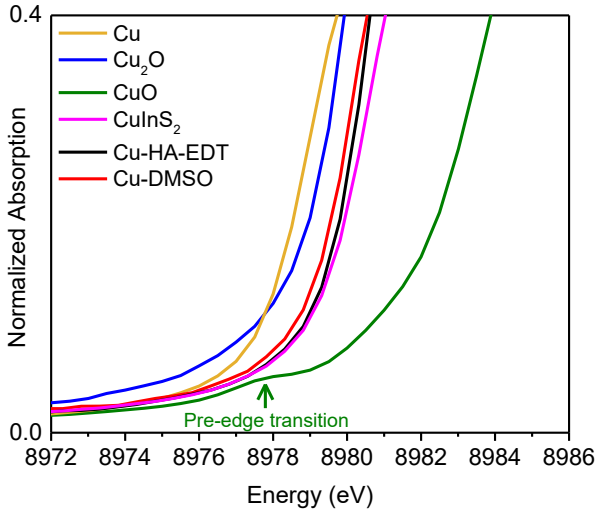

Figure 2. Cu K-edge XANES spectra for 0.1 M Cu in HA-EDT solution and 0.1 M Cu complex in DMSO solution along with Cu foil, CuO, Cu_2O and $CuInS_2$ references (focused near edge energy).

The Fourier transforms of k^3-weighted Cu K-edge spectrum for Cu-HA-EDT are shown in Figure S8 and the curve fittings are carried out to these EXAFS oscillations. The best fitting results to the Fourier filtered first coordination shell are compared with the experimental data, and the fitted structural parameters are listed in Table 3. The average bond distance for Cu in Cu-HA-EDT is 2.24 Å, which is close to the value of Cu-S bond length 2.34 Å in $CuInS_2$ reported previously.[32] The average coordination number for Cu obtained through this analysis is 3.0, suggesting that 3 sulfur atoms are surrounding the Cu^+ cation in Cu-HA-EDT sample.

Table 3. Structural parameters obtained from the best fits to Cu HA-EDT spectrum at the Cu K edge

Sample	C.N.	*R* (Å)	σ^2 (Å^2)	E_0 (eV)
Cu-HA-EDT	3.0	2.24	0.005	3.0
Cu-DMSO	3.0	2.29	0.01	6.0

C.N.: Coordination Number, R: Interatomic distance, E_0: Shift in threshold energy, σ^2: Debye–Waller factor squared, S_0^2: Intrinsic loss factor, S_0^2 = 1.0.

Further analysis of Cu complex species in Cu-HA-EDT solutions was performed with ESI-MS analysis. The negative mode mass spectrometry was performed on the Cu-HA-EDT solution diluted with acetonitrile solvent, resulting in the spectrum shown in Figure S9. Unlike In-HA-EDT complex, Cu-HA-EDT complex indicates the presence of multiple ions containing copper's isotopic pattern in the negative ion spectrum. Table S2 lists all the ionized molecules which are observed in significant quantities (relative abundance > 15%) in the spectrum and their proposed chemical composition. Based on this chemical composition and the difference between m/z of the peaks observed in negative ESI-MS data, which could be a result of fragmentation process, linear arrangements of copper thiolate structures corresponding to each peak are shown in Table S2. The most significant species observed in this analysis having m/z values of 530.65, 594.57 and 812.41, etc. suggests presence of high nuclearity Cu (I) thiolate clusters (number of Cu atoms = 2~8 in the molecule). Similar Cu clusters are commonly observed in proteins with a large number of variations and types in previously reported articles[35]. Due to the $3d^{10}$ configuration of cuprous copper, complexes with diagonal two-coordinate linear coordination, trigonal three coordinate planar coordination, and pseudo tetrahedral geometries are known[36]. Supported by the spatial confinement of 1,2-ethanedithiol molecules and previous reports on Cu-dithiolate structures[37], it is believed that the Cu (I) thiolate clusters shown in Table S2 could likely exhibit compact configurations in solution instead of linear, open arrangements. Although Cu is coordinated to 2 S atoms in most of the proposed linear structures in Table S2, the compact arrangement of copper clusters could result in an interaction between Cu and another S atom in the cluster resulting in an average CN close to 3 as observed in XAS analysis. Figure 3 shows a possible representation of linear and compact cluster for the most abundant peak (m/z = 594.57) in negative ESI-MS data of copper complex.

Figure 3. Proposed (a) linear and (b) compact cluster structures for copper complex with m/z of 594.57.

These results are also in agreement with the structures and XAS data reported by Murria et al. in the case of CuCl and $CuCl_2$ dissolution in butylamine and propanethiol solutions.[38] Specifically the structure proposed by Murria et al. for a peak corresponding to m/z of 769 in negative ion ESI-MS of copper chloride solutions through computational analysis show similar arrangement of Cu and S atoms as proposed in Figure 3b cluster.

Similar to In-HA-EDT sample, positive mode mass spectrometry of Cu-HA-EDT shows multiple peaks without any presence of copper's isotopic pattern (Figure S10). Table S3 compiles all the peaks and possible chemical composition for these cations, which suggests complex amine coordination forming secondary and tertiary amine structures. Based on the In-HA-EDT analysis, it is thought that similar ionic reactions could occur during the ionization of Cu-HA-EDT in the mass spectrometer giving the observed results.

Unlike In complex, the Cu complex is insoluble in acetonitrile, so NMR analysis of Cu-HA-EDT solution was performed using DMSO-d6 solvent. Both ^{13}C-NMR (Figure S11) and ^{1}H-

NMR (Figure S12) show multiple peaks which do not correspond to the hexylammonium ion. Although the interpretation and assignment for these peaks is not certain, their presence and corresponding interaction detected by 2D ^{1}H-^{13}CNMR (Figure S13) supports the presence of multiple Cu thiolate structures in the solution.

3.1.3 Gas Product Analysis: Dissolution of pure metals (e.g In, Cu, Zn, etc.) in amine-thiol (monoamine-monothiol, monoamine-dithiol, diamine-dithiol) solution generates a gaseous product along with heat, suggesting an exothermic nature of this reactive dissolution. The gaseous products released during dissolutions were analyzed using thermal conductivity detection (TCD)-mass spectrometry (MS). As an example, gas generated from In-HA-EDT solution was collected using a syringe in a N_2 filled glovebox. N_2 was also used as the carrier gas for the TCD-MS measurement. The TCD results are shown in Figure 4. At 17 min, 1 mL of pure H_2 gas (99.999%) was injected as a reference, and then a large positive peak signal was observed in the curve. At 24 min, 1 mL of the collected gas product was injected into the system, and another large positive signal was observed. The TCD compares the thermal conductivities of two gas flows – pure carrier gas (N_2), and carrier gas plus sample components (column effluent). Since the thermal conductivity of H_2 (186.9 mW/mK, T = 300 K) is much higher than that of N_2 (26.0 mW/mK, T = 300 K), when H_2 flow elutes from the column the effluent thermal conductivity is increased, and a positive signal is observed. In contrast, at 27 min, 1 mL of pure Ar gas (99.999 %) was injected, and a small negative signal was detected, due to the relatively low thermal conductivity of Ar (17.9 mW/mK) as compared with N_2. Only very few gases (H_2, He, and Ne) have higher thermal conductivity than that of N_2. In order to exclude the low possibility of He or Ne gases, MS was coupled with TCD to analyze the gas composition after the gas sample passed the TCD column. No He or Ne peak was observed on this spectrum. Therefore, it can be concluded that H_2 is generated during metal dissolution reaction in HA-EDT solution.

Figure 4. TCD signal of the gas products of the In dissolution reaction in HA-EDT solution.

Based on detailed analysis of In thiolate species and the gaseous products, the proposed reaction for In in amine-dithiol is shown in Scheme 1. The initial step shown in the scheme suggests formation of ionic liquid via proton transfer after mixing amine and dithiol together without any metal. The rise in ionic conductivity of the solution after mixing amine and dithiol together has already been demonstrated in literature[17]. The FTIR analysis performed on pure amine and pure dithiol solutions before and after mixing (Figure S14) also supports this proton transfer mechanism, as the SH stretching from dithiol (2552 cm^{-1}) and symmetric/antisymmetric N-H peaks from primary amine (3290, 3370 cm^{-1}) disappear after mixing HA and EDT in 2:1 mole ratio.

Scheme 1: Proposed dissolution pathway for In metal in amine-dithiol solution.

3.2 Dissolution of Metal Complexes in Benign Solvents

According to the proposed mechanism of metal dissolution in the amine-thiol system, it is clear that the reaction between precursors is irreversible due to the release of H_2 gas, which allows us to isolate the metal thiolates from the solution by evaporation. As amine-thiol is capable of dissolving various metals, the precursor ink presents material compatibility challenges during its handling and possible scale up. So, the ability to isolate metal thiolates from amine-thiol solutions and re-dissolve them in benign solvents provides a route for minimizing the reactivity and toxicity associated with the precursor ink.

As mentioned in XAS analysis, the isolated Cu and In thiolates are soluble in solvents like DMSO at high concentrations. Along with solubility, these solutions are also stable (without any solid precipitation) for days, giving sufficient time for their processing. Along with DMSO, other benign and weakly coordinating solvents can also be used to dissolve isolated metal thiolate species. Figure 5 summarizes various solvents that were tested for thiolate dissolution. As can be seen from Figure 5a, Cu thiolate solutions in acetone and THF appear cloudy when compared to other Cu solutions. These two solutions remained cloudy even with further dilution, suggesting presence of insoluble species in the solution. Further analysis performed after filtering these solutions confirms the presence of Cu in filtrate as well as in the insoluble residue (Figure S15). This implies the selective dissolution of Cu thiolate species in these solvents. Although acetone and THF partially dissolved Cu thiolate species, solvents like DMSO, DMF and 2-methoxyethanol were able to dissolve Cu thiolates completely. Similar to Cu and In thiolates, the isolated Se complex was also found to be soluble in multiple benign solvents. Use of these benign processing reagents for the deposition of metal chalcogenides might help minimize the carbon impurities in the thin films and overcome many other disadvantages of established amine-thiol approaches. The thiolate salts of other metals such as Zn, Sn, and Ga with Se dissolved in amine-thiol can also be isolated and redissolved in different benign solvents (Figure S16) for the broad applicability of this new approach.

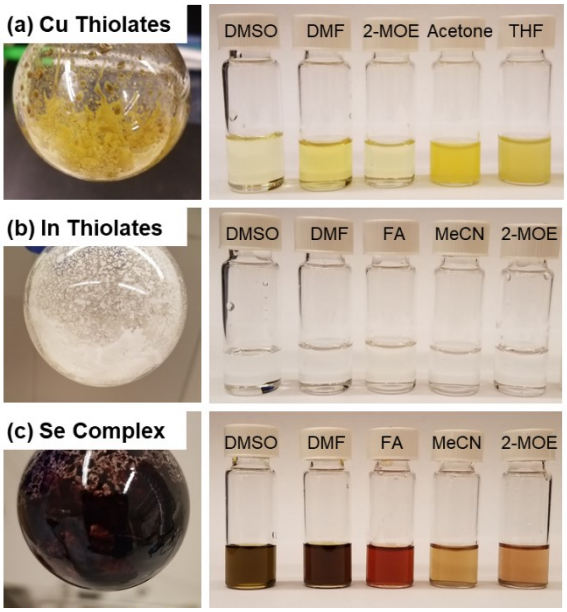

Figure 5. Photographs of (a) Cu thiolates, (b) In thiolates, and (c) Se complex dissolved in different types of benign solvents. (DMSO-dimethyl sulfoxide, DMF-dimethylformamide, FA-formamide, MeCN-acetonitrile, 2-MOE-2-methoxyethanol, THF-tetrahydrofuran)

3.3 Film Fabrication and Characterization

Amongst various solvents used for metal thiolate dissolutions, DMSO gave higher solubility for Cu and In thiolates (>0.5M). This higher concentration of ink can provide the desired film thickness in fewer coating steps making DMSO an attractive solvent for film deposition. In addition, XAS analysis performed on metal thiolate solutions confirmed that the oxidation state and coordination environment of Cu and In in their corresponding metal thiolates remain unchanged in presence of DMSO, so DMSO was selected as the solvent for film fabrication. Se incorporation in this ink was realized by adding Se-DMSO ink to the Cu-In-DMSO ink at an optimized (Cu+In):Se ratio of 1:0.1 which enabled a micron thick crack-free film fabrication with minimal number of coating steps. The film fabrication temperature required for complete removal of solvents was chosen to be 330 °C based on the results obtained from TGA analysis (Figure S17). Fabricated films were then selenized in a selenium-rich atmosphere at 500 °C in a tube furnace apparatus to yield desired bandgap absorber material. Figures 5a and 5c show Raman and XRD data obtained for selenized film confirming the phase purity of the material. The strong and narrow Raman peak at 174 cm^{-1} corresponds to the A1 vibration mode of $CuInSe_2$ while the small peaks at 212 cm^{-1} and 230 cm^{-1} are assigned to B2 and E vibration modes. The XRD pattern of selenized CISSe film matches closely with the standard $CuInSe_2$ (ICSD collection code 73351) chalcopyrite structure with slight shift towards higher 2θ, suggesting presence of residual $CuInS_2$ due to incomplete conversion of sulfides to selenides.

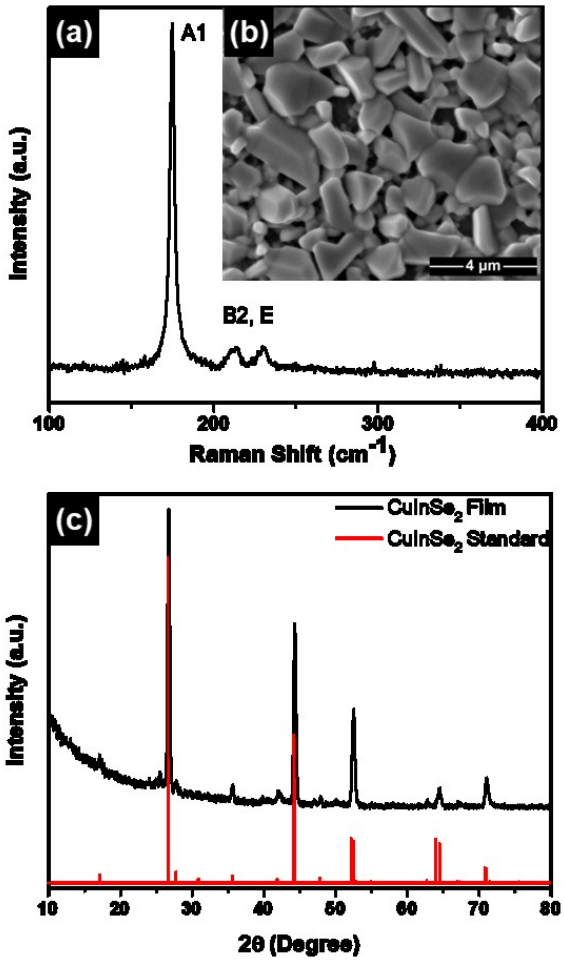

Figure 6. (a) Raman spectrum, (b) top view SEM image and (c) XRD pattern of selenized CISSe film fabricated using DMSO ink.

The selenized film is then used to fabricate photovoltaic devices by depositing CdS, i-ZnO, ITO and Ni/Al grids as described in the experimental section. The current-voltage characteristics of devices fabricated using DMSO ink were obtained under AM 1.5 illumination with after 20 min. of light soaking and depositing 100 nm anti-reflective MgF_2 coating. The best device efficiency of 9.03% based on total area of 0.472 cm^2 (including grid area) was achieved for this film. Open circuit voltage, current density and fill factor of 450 mV, 34.5 mA/cm^2 and 58.1% were recorded for the champion device. The corresponding J-V curve for this device is shown in Figure 7a and the active area (0.44 cm^2) efficiency for same device was calculated to be 9.7%.

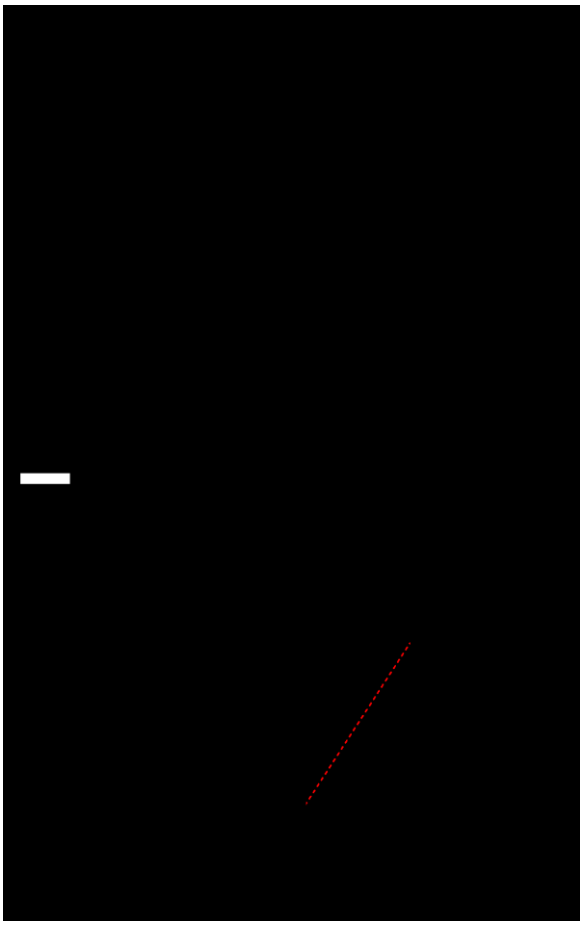

Figure 7. (a) Electrical characteristics of CISSe solar cell (total device area: 0.452 cm^2). (AM 1.5G illumination with light soaking for 20min; 100mWcm^{-2}; the Ni/Al grid-covered area is included in the total device area) (b) External quantum efficiency (EQE) spectrum of the CISSe device. The insert is a bandgap determination from near band edge section of the EQE.

For further device characterization, external quantum efficiency (EQE) measurements were performed under zero bias conditions. As can be seen from Figure 7b, quantum efficiencies obtained from these measurements are above 80% in the visible wavelength range. The bandgap calculated from this EQE data is around 1.02 eV (insert of Figure 7b). This slightly higher bandgap compared to the expected 1 eV value can be attributed to incomplete conversion of $CuInS_2$ to $CuInSe_2$ in the process of selenization.

Based on J-V analysis in reverse bias, the shunt resistances were found to be 129 ohm/cm^2 in light and 125 ohm/cm^2 in dark. These values for shunt resistances are an order of magnitude lower than high efficiency CIGSe devices. Such lower shunt resistance affects the overall efficiency of the device by introducing current loss and reducing the fill factor of the device. Origin of shunting in these devices could be attributed to the presence of pinholes in the final selenized film as can be seen from top-view SEM image shown in Figure 6b. Demonstration of CISSe efficiencies above 9% even with significant shunting pathways promises enough room for further improvement in the device performance by film processing optimization.

Conclusion

The dissolution mechanism for elemental metals in a mono-amine-dithiol solution is studied. The metal complexes formed as a product of dissolution were isolated from the solution by evaporating unreacted solvents and were analyzed using XAS, ESI-MS, and NMR and are hypothesized to be bis(1,2-ethanedithiolate) indium (III) in the case of indium dissolution and high nuclearity Cu (I) thiolate compounds in the case of copper dissolution. It was found that the metal dissolution releases H_2 gas while oxidizing metals to average oxidation states of +1 and +3 for Cu and In, respectively. The isolated metal thiolates were shown to be soluble in various benign solvents, amongst which DMSO was further employed for film fabrication. XAS analysis performed on thiolate-DMSO solutions confirmed the absence of any interaction between metals and DMSO, enabling phase pure CISSe film fabrication. A preliminary photovoltaic device fabricated from this low bandgap (~ 1.02 eV) CISSe absorber yielded a power conversion efficiency of 9.03%. Optimization of film fabrication towards pinhole free film with this newly developed benign ink system promises further improvement in device performance. Demonstration of metal thiolate isolation for metals Cu, In, Zn, Sn, and Ga with Se and their redissolution in different benign solvents shows the versatility of this new approach for semiconductor thin film fabrication.

ASSOCIATED CONTENT

Supporting Information.
Fourier transforms (FTs) of In and Cu K-edge EXAFS spectra, positive and negative mode ESI-MS spectra and data for In-HA-EDT and Cu-HA-EDT samples, NMR data for In-HA-EDT and Cu-HA-EDT samples, FTIR data for HA, EDT and HA+EDT, pictures of Zn, Sn and Ga with Se thiolates and their inks in various solvents, TGA data on new CISSe-DMSO ink. This material is available free of charge via the Internet at http://pubs.acs.org.

AUTHOR INFORMATION

Corresponding Author

*E-mail: agrawalr@purdue.edu

Author Contributions

† X. Zhao and S. D. Deshmukh contributed equally to this work.

ACKNOWLEDGMENT

XZ and SDD were supported in part by NSF under the grant #1534691-DMR (DMREF) and DJR was supported by NSF under the grant #1735282-NRT (SFEWS). GZ, ZW and JTM were supported in part by the NSF under Cooperative Agreement No. EEC-1647722. GZ would also like to acknowledge the Fundamental Research Funds for the Central Universities (DUT18RC(3)057). Use of the Advanced Photon Source was supported by the U.S. Department of Energy, Office of Basic Energy Sciences, under contract no. DE-AC02-06CH11357. MRCAT operations, beamline 10-BM, are supported by the Department of Energy and the MRCAT member institutions. Authors would also like to acknowledge Aron Perfect for his help with metal thiolate isolation experiments, Yanran Cui for TCD-MS measurements, Nicole Libretto for discussions on X-ray absorption analysis and Essam Alruqobah, Xianyi Hu and Joseph Andler for their assistance and expertise in preparing molybdenum coated soda lime glass substrate.

REFERENCES

(1) Rau, U.; Schock, H. W. Electronic Properties of $Cu(In,Ga)Se_2$ Heterojunction Solar Cells-Recent Achievements, Current Understanding, and Future Challenges. *Appl. Phys. A Mater. Sci.*

Process. **1999**, *69* (2), 131–147.

(2) Jehad AbuShama; Noufi, R.; Johnston, S.; Ward, S.; Wu, X. Improved Performance in $CuInSe_2$ and Surface-Modified $CuGaSe_2$ Solar Cells. In *Conference Record of the Thirty-first IEEE Photovoltaic Specialists Conference, 2005.*; IEEE, **2005**, 299–302.

(3) Kato, T.; Wu, J.; Hirai, Y.; Sugimoto, H.; Bermudez, V. Record Efficiency for Thin-Film Polycrystalline Solar Cells Up to 22.9% Achieved by Cs-Treated $Cu(In,Ga)(Se,S)_2$. *IEEE J. Photovoltaics* **2019**, *9* (1), 325–330.

(4) Hossain, M. A.; Tianliang, Z.; Keat, L. K.; Xianglin, L.; Prabhakar, R. R.; Batabyal, S. K.; Mhaisalkar, S. G.; Wong, L. H. Synthesis of $Cu(In,Ga)(S,Se)_2$ Thin Films Using an Aqueous Spray-Pyrolysis Approach, and Their Solar Cell Efficiency of 10.5%. *J. Mater. Chem. A* **2015**, *3* (8), 4147–4154.

(5) Uhl, A. R.; Katahara, J. K.; Hillhouse, H. W. Molecular-Ink Route to 13.0% Efficient Low-Bandgap $CuIn(S,Se)_2$ and 14.7% Efficient $Cu(In,Ga)(S,Se)_2$ Solar Cells. *Energy Environ. Sci.* **2016**, *9* (1), 130–134.

(6) Park, S. J.; Cho, J. W.; Lee, J. K.; Shin, K.; Kim, J.-H.; Min, B. K. Solution Processed High Band-Gap $CuInGaS_2$ Thin Film for Solar Cell Applications. *Prog. Photovoltaics Res. Appl.* **2014**, *22* (1), 122–128.

(7) Septina, W.; Kurihara, M.; Ikeda, S.; Nakajima, Y.; Hirano, T.; Kawasaki, Y.; Harada, T.; Matsumura, M. $Cu(In,Ga)(S,Se)_2$ Thin Film Solar Cell with 10.7% Conversion Efficiency Obtained by Selenization of the Na-Doped Spray-Pyrolyzed Sulfide Precursor Film. *ACS Appl. Mater. Interfaces* **2015**, *7* (12), 6472–6479.

(8) Wang, W.; Han, S.-Y.; Sung, S.-J.; Kim, D.-H.; Chang, C.-H. 8.01% $CuInGaSe_2$ Solar Cells Fabricated by Air-Stable Low-Cost Inks. *Phys. Chem. Chem. Phys.* **2012**, *14* (31), 11154.

(9) Weil, B. D.; Connor, S. T.; Cui, Y. $CuInS_2$ Solar Cells by Air-Stable Ink Rolling. *J. Am. Chem. Soc.* **2010**, *132* (19), 6642–6643.

(10) Xie, Y.; Chen, H.; Li, A.; Zhu, X.; Zhang, L.; Qin, M.; Wang, Y.; Liu, Y.; Huang, F. A Facile Molecular Precursor-Based $Cu(In,Ga)(S,Se)_2$ Solar Cell with 8.6% Efficiency. *J. Mater. Chem. A* **2014**, *2* (33), 13237.

(11) Wang, G.; Wang, S.; Cui, Y.; Pan, D. A Novel and Versatile Strategy to Prepare Metal–Organic Molecular Precursor Solutions and Its Application in $Cu(In,Ga)(S,Se)_2$ Solar Cells. *Chem. Mater.* **2012**, *24* (20), 3993–3997.

(12) Zhao, W.; Cui, Y.; Pan, D. Air-Stable, Low-Toxicity Precursors for $CuIn(SeS)_2$ Solar Cells with 10.1% Efficiency. *Energy Technol.* **2013**, *1* (2–3), 131–134.

(13) Mitzi, D. B.; Yuan, M.; Liu, W.; Kellock, A. J.; Chey, S. J.; Deline, V.; Schrott, A. G. A High-Efficiency Solution-Deposited Thin-Film Photovoltaic Device. *Adv. Mater.* **2008**, *20* (19), 3657–3662.

(14) Liu, W.; Mitzi, D. B.; Yuan, M.; Kellock, A. J.; Chey, S. J.; Gunawan, O. 12% Efficiency $CuIn(Se,S)_2$ Photovoltaic Device Prepared Using a Hydrazine Solution Process. *Chem. Mater.* **2010**, *22* (3), 1010–1014.

(15) Zhang, T.; Yang, Y.; Liu, D.; Tse, S. C.; Cao, W.; Feng, Z.; Chen, S.; Qian, L. High Efficiency Solution-Processed Thin-Film $Cu(In,Ga)(Se,S)_2$ Solar Cells. *Energy Environ. Sci.* **2016**, *9* (12), 3674–3681.

(16) Zhao, D.; Tian, Q.; Zhou, Z.; Wang, G.; Meng, Y.; Kou, D.; Zhou, W.; Pan, D.; Wu, S. Solution-Deposited Pure Selenide CIGSe Solar Cells from Elemental Cu, In, Ga, and Se. *J. Mater. Chem. A* **2015**, *3* (38), 19263–19267.

(17) Zhang, R.; Cho, S.; Lim, D. G.; Hu, X.; Stach, E. A.; Handwerker, C. A.; Agrawal, R. Metal–metal Chalcogenide Molecular Precursors to Binary, Ternary, and Quaternary Metal Chalcogenide Thin Films for Electronic Devices. *Chem. Commun.* **2016**, *52* (28), 5007–5010.

(18) Buckley, J. J.; McCarthy, C. L.; Del Pilar-Albaladejo, J.; Rasul, G.; Brutchey, R. L. Dissolution of Sn, SnO, and SnS in a Thiol–Amine Solvent Mixture: Insights into the Identity of the Molecular Solutes for Solution-Processed SnS. *Inorg. Chem.* **2016**, *55* (6), 3175–3180.

(19) Walker, B. C.; Agrawal, R. Contamination-Free Solutions of Selenium in Amines for Nanoparticle Synthesis. *Chem. Commun.* **2014**, *50* (61), 8331–8334.

(20) Webber, D. H.; Buckley, J. J.; Antunez, P. D.; Brutchey, R. L. Facile Dissolution of Selenium and Tellurium in a Thiol–amine Solvent Mixture under Ambient Conditions. *Chem. Sci.* **2014**, *5* (6), 2498.

(21) Yang, Y.; Wang, G.; Zhao, W.; Tian, Q.; Huang, L.; Pan, D. Solution-Processed Highly Efficient $Cu_2ZnSnSe_4$ Thin Film Solar Cells by Dissolution of Elemental Cu, Zn, Sn, and Se Powders. *ACS Appl. Mater. Interfaces* **2015**, *7* (1), 460–464.

(22) Qi, Y.; Tian, Q.; Meng, Y.; Kou, D.; Zhou, Z.; Zhou, W.; Wu, S. Elemental Precursor Solution Processed $(Cu_{1-X}Ag_X)_2ZnSn(S,Se)_4$ Photovoltaic Devices with over 10% Efficiency. *ACS Appl. Mater. Interfaces* **2017**, *9* (25), 21243–21250.

(23) McCarthy, C. L.; Brutchey, R. L. Solution Deposited $Cu_2BaSnS_{4-x}Se_x$ from a Thiol-Amine Solvent Mixture. *Chem. Mater.* **2018**, *30* (2), 304–308.

(24) McCarthy, C. L.; Webber, D. H.; Schueller, E. C.; Brutchey, R. L. Solution-Phase Conversion of Bulk Metal Oxides to Metal Chalcogenides Using a Simple Thiol-Amine Solvent Mixture. *Angew. Chemie Int. Ed.* **2015**, *54* (29), 8378–8381.

(25) Webber, D. H.; Brutchey, R. L. Alkahest for V_2VI_3 Chalcogenides: Dissolution of Nine Bulk Semiconductors in a Diamine-Dithiol Solvent Mixture. *J. Am. Chem. Soc.* **2013**, *135* (42), 15722–15725.

(26) Zhao, X.; Lu, M.; Koeper, M. J.; Agrawal, R. Solution-Processed Sulfur Depleted $Cu(In,Ga)Se_2$ Solar Cells Synthesized from a Monoamine–dithiol Solvent Mixture. *J. Mater. Chem. A* **2016**, *4* (19), 7390–7397.

(27) Zhang, R.; Szczepaniak, S. M.; Carter, N. J.; Handwerker, C. A.; Agrawal, R. A Versatile Solution Route to Efficient $Cu_2ZnSn(S,Se)_4$ Thin Film Solar Cells. *Chem. Mater.* **2015**, *27* (6), 2114–2120.

(28) Nelson, R. C.; Miller, J. T. An Introduction to X-Ray Absorption Spectroscopy and Its in Situ Application to Organometallic Compounds and Homogeneous Catalysts. *Catal. Sci. Technol.* **2012**, 2, 461–470.

(29) Guo, Q.; Ford, G. M.; Hillhouse, H. W.; Agrawal, R. Sulfide Nanocrystal Inks for Dense $Cu(In_{1-X}Ga_X)(S_{1-Y}Se_Y)_2$ Absorber Films and Their Photovoltaic Performance. *Nano Lett.* **2009**, *9* (8), 3060–3065.

(30) Ravel, B.; Newville, M. ATHENA, ARTEMIS, HEPHAESTUS: Data Analysis for X-Ray Absorption Spectroscopy Using IFEFFIT. *J. Synchrotron Radiat.* **2005**, *12* (4), 537–541.

(31) Yao, J.; Rudyk, B. W.; Brunetta, C. D.; Knorr, K. B.; Figore, H. A.; Mar, A.; Aitken, J. A. Mn Incorporation in $CuInS_2$ Chalcopyrites: Structure, Magnetism and Optical Properties. *Mater. Chem. Phys.* **2012**, *136* (2–3), 415–423.

(32) S. C. Abrahams and J. L. Bernstein. Piezoelectric Nonlinear Optic $CuGaS_2$ and $CuInS_2$ Crystal Structure: Sublattice Distortion in $A^IB^{III}C_2^{VI}$ and $A^{II}B^{IV}C_2^{V}$ Type Chalcopyrites. *J. Chem. Phys.* **1973**, *59* (10), 5415-5422.

(33) Michael Lappert, Andrey Protchenko, Philip Power, A. S. *Metal Amide Chemistry*; Wiley, 2009.

(34) González, G. B. Investigating the Defect Structures in Transparent Conducting Oxides Using X-Ray and Neutron Scattering Techniques. *Materials (Basel).* **2012**, *5* (12), 818–850.

(35) Pickering, I. J.; George, G. N.; Dameron, C. T.; Kurz, B.; Winge, D. R.; Dance, I. G. X-Ray Absorption Spectroscopy of Cuprous-Thiolate Clusters in Proteins and Model Systems. *J. Am. Chem. Soc.* **1993**, *115* (21), 9498–9505.

(36) Pushie, M. J.; Zhang, L.; Pickering, I. J.; George, G. N. The Fictile Coordination Chemistry of Cuprous-Thiolate Sites in Copper Chaperones. *Biochim. Biophys. Acta - Bioenerg.* **2012**, *1817* (6), 938–947.

(37) Rao, C. P.; Dorfman, J. R. Synthesis and Structural Systematics of Ethane-1 , 2-Dithiolato Complexes. *Inorg. Chem.* **1986**, *25* (4), 428–439.

(38) Murria, P.; Miskin, C. K.; Boyne, R.; Cain, L. T.; Yerabolu, R.; Zhang, R.; Wegener, E. C.; Miller, J. T.; Kenttämaa, H. I.; Agrawal, R. Speciation of CuCl and $CuCl_2$ Thiol-Amine Solutions and Characterization of Resulting Films: Implications for Semiconductor Device Fabrication. *Inorg. Chem.* **2017**, *56* (23), 14396–14407.

Table of Contents Graphic